

Three-dimensional optical lattice clock with bosonic ^{88}Sr atomsTomoya Akatsuka,^{1,2,*} Masao Takamoto,^{1,2} and Hidetoshi Katori^{1,2}¹*Department of Applied Physics, Graduate School of Engineering, The University of Tokyo, Bunkyo-ku, Tokyo 113-8656, Japan*²*CREST, Japan Science and Technology Agency, 4-1-8 Honcho Kawaguchi, Saitama 332-0012, Japan*

(Received 4 July 2009; published 4 February 2010)

We present detailed analyses of our recent experiment on the three-dimensional (3D) optical lattice clock with bosonic ^{88}Sr atoms in which the collisional frequency shift was suppressed by applying a single-occupancy lattice. Frequency shifts in magnetically induced spectroscopy on the $^1S_0\text{-}^3P_0$ clock transition ($\lambda = 698$ nm) of ^{88}Sr were experimentally investigated by referencing a one-dimensional (1D) lattice clock based on spin-polarized ^{87}Sr atoms. We discuss that the clock stability is limited by the current laser stability as well as the experimental sequence of the clock operation, which may be improved to $\sigma_y(\tau) = 2 \times 10^{-16}/\sqrt{\tau}$ by optimizing the cycle time of the clock operation.

DOI: [10.1103/PhysRevA.81.023402](https://doi.org/10.1103/PhysRevA.81.023402)

PACS number(s): 37.10.Jk, 32.80.Qk, 06.30.Ft

I. INTRODUCTION

Quantum absorbers singly trapped in a region much smaller than the relevant transition wavelengths are free from Doppler and collisional shifts; therefore, they are considered to be promising resources for optical clocks [1,2] that allow better stability and accuracy than those of the state-of-the-art Cs fountain clocks [3,4]. To date, the fractional uncertainty of 5.2×10^{-17} was demonstrated by measuring the frequency ratio of two single-ion optical clocks using Al^+ and Hg^+ ions operated close to their quantum-projection-noise-limited stabilities [5]. An optical lattice clock was proposed [6,7] to attain better stability by employing millions of atoms trapped in well-engineered optical lattices. The relevant light shifts can be removed down to the 10^{-18} uncertainty, including atomic multipolar effects [8], by operating the clock on the $^1S_0\text{-}^3P_0$ scalar states that minimize the vector as well as tensor light shift [7]. Since the first demonstration [9,10] of the scheme, optical lattice clocks were demonstrated with one-dimensional (1D) optical lattices employing fermionic [11–17] or bosonic [18–21] isotopes, highlighting their narrow Doppler-free spectrum. Until now absolute frequency measurements of optical lattice clocks were carried out at the Cs clocks' uncertainty limit in the JILA [15], LNE-SYRTE [14], National Institute of Standards and Technology (NIST) [16] groups and a team of the University of Tokyo and National Metrology Institute of Japan (NMIJ) groups [22].

Used with multiple atoms trapped in each site of a 1D lattice, the collisional frequency shift can be a serious concern as the precision of the clock improves. To tackle the issue, Pauli blocking of collisions [23,24] were explored using spin-polarized fermions [13,14,25]. Nonzero collision shift was observed by the JILA group [25] with fermionic atoms when the spin polarization was degraded due to atomic-motion-sensitive clock excitation. By carefully aligning the clock laser with the 1D lattice so as to be insensitive to atomic transverse motion, a very high degree (>98%) of spin polarization in the clock excitation was demonstrated in the Tokyo group [26]. It was predicted theoretically that the collisional shift can

be reduced down to $10^{-17}\text{--}10^{-18}$ uncertainty for an experimentally feasible spin polarization [27]. For bosons multiply trapped in each site of a 1D lattice the collisional frequency shift is unavoidable; the collisional losses and frequency shifts on the clock transition were systematically investigated in the Physikalisch-Technische Bundesanstalt (PTB) group [21].

These studies with fermionic as well as bosonic 1D clocks indicate that a single-occupancy three-dimensional (3D) optical lattice, as assumed in the original proposal [6,7], may provide a robust means for realizing optical lattice clocks free from the collision shift. In contrast to 1D lattices, in 3D lattices, however, the light polarization of the lattice cannot be spatially uniform, which makes the coupling of the clock states with the local lattice polarizations problematic, especially for fermionic isotopes with nonzero angular momentum [7]. In the bosonic isotope, as a result of the purely scalar nature of the $^1S_0\text{-}^3P_0$ clock states, their coupling to the lattice-field polarization is solely introduced by an external mixing field [28,29] that is necessary for a magnetically induced spectroscopy and is experimentally controllable [30].

Recently we demonstrated the frequency comparison between a 3D lattice clock with bosonic ^{88}Sr and a 1D lattice clock with fermionic ^{87}Sr [31], both of which represent the noninteracting atomic samples. In this article, we present a detailed description of the 3D optical lattice clock with bosonic ^{88}Sr , which have not been reported in depth so far. In particular, we describe the evaluation of uncertainties for the lattice polarization effects and for the collision shift, both of which are the specific features in the 3D bosonic lattice clock. Furthermore, the stability of the clock is discussed in detail: The Dick-effect-limited stability calculated for our laser noise spectrum well explains the measured stability, which may be improved to 2×10^{-16} for 1 s by reducing the clock cycle time down to 0.1 s. To present unified aspects of the bosonic 3D clock we use previously published results [31] when necessary.

This article is organized as follows. Section II describes the 3D optical lattice used in the experiment. The spectroscopy on the magnetically induced clock transition is given in Sec. III. Section IV describes the frequency evaluation referencing the fermionic 1D clock and discusses the Dick effect that limits stability of the measurements. An evaluation of uncertainties is given in Sec. V. Finally, we address future work in Sec. VI, including the feasibility of applying fermionic isotopes to

*Present address: Faculty of Science and Technology, Tokyo University of Science, Noda shi, Chiba 278-8510, Japan

3D lattices. The Appendix discusses the lattice polarization rotation effects for atoms oscillating in the lattice site, which may be a concern in applying fermionic ^{87}Sr atoms to the 3D lattice.

II. A 3D OPTICAL LATTICE

To suppress atomic collisions and to confine atoms in the Lamb-Dicke regime, it is straightforward to apply 3D optical lattices with less than a single atom in each lattice site [6], which is of particular importance in employing bosonic isotopes as interrogated atoms because of their bunching nature that may introduce collision shifts. In view of recent advances in creating Bose-Einstein condensates (BEC) in alkaline-earth-metal (-like) species, such as Yb [32], ^{40}Ca [33], and ^{84}Sr [34,35], the Mott-insulator state [36] with a single atom in each lattice site that is made of BEC will allow attaining dense lattices to further improve clock stability. Moreover, in the 3D configuration, blue-detuned optical lattices [37] that reduce the higher-order light shift are applicable.

Technically, however, it is more challenging to realize a stable 3D optical lattice than 1D ones, as the 3D lattice requires four or more laser beams and, in addition, their relative phases critically affect the position and the local polarization of the lattice sites [38]. Instead of actively stabilizing the relative time phase of the lattice beams, we employed an intrinsically phase-stable configuration, the so-called “folded optical lattice” [39] where an n -dimensional optical lattice is formed by a single standing wave, which is viewed as the natural extension of a 1D lattice with a retro-reflected beam.

We constructed an orthogonally crossed “folded” 3D optical lattice in an optical enhancement cavity, as shown in Fig. 1. Taking advantage of the cavity enhancement of the coupled laser power, we designed the lattice to have relatively large volume with modest potential depth to load as many atoms into the lattice as possible. The intracavity laser power P_{cav} is given by $P_{\text{cav}} = P_{\text{in}}(1 - R)/[1 - \sqrt{R}(1 - L)]^2$, where P_{in} is the laser power coupling into the cavity, R is the reflectivity of the input coupling mirror, and L is the round trip loss in the cavity. The maximum enhancement of $1/L$ can be obtained by setting $R = 1 - L$. In our cavity, all the cavity mirrors except the input coupling mirror were set inside the vacuum chamber to minimize the cavity loss. The round trip loss of the cavity was estimated to be $L = 0.063$ including the transmission of the vacuum window ($T = 0.99$) and the reflectivity $R_m = 0.995$ of each cavity mirror. We thus used an input coupling mirror with $R = 1 - L = 0.935(5)$ and obtained the enhancement of $P_{\text{cav}}/P_{\text{in}} = 14$. The lattice cavity length was 630 mm and the cavity linewidth was 5 MHz.

By tuning the lattice laser to the “magic wavelength,” the differential light shift in the 1S_0 - 3P_0 clock transition can be removed to the second order in the electric dipole interaction. A precise definition of the “magic wavelength” including the multipolar interactions of atoms with lattice field is discussed elsewhere [8]. The “magic wavelength” lattice laser at $\lambda_L = 813.42$ nm was generated by a master oscillator and power amplifier (MOPA) system using an external cavity diode laser (ECDL) as a master oscillator, electronically stabilized to a reference cavity with a linewidth of 140 kHz. Typically, the lattice laser power of $P_{\text{in}} = 140$ mW was coupled into the

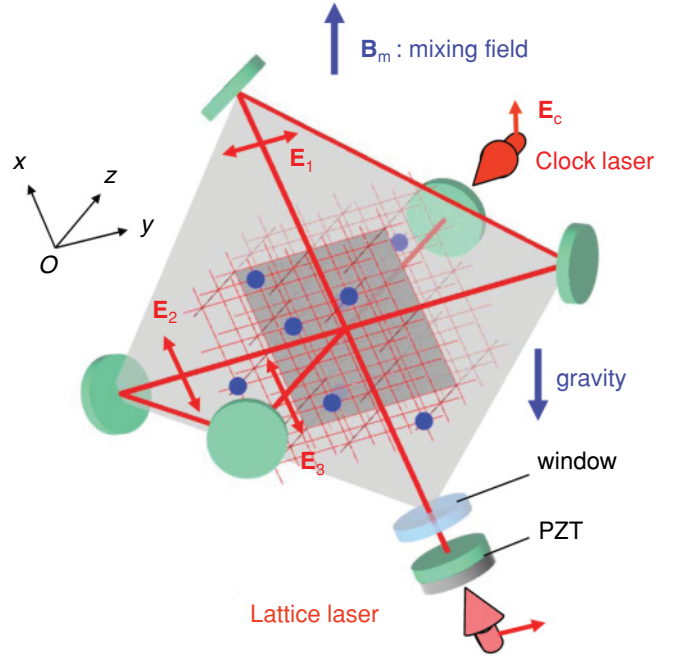


FIG. 1. (Color online) A 3D optical lattice is realized in the optical enhancement cavity whose mirrors are placed inside a vacuum chamber except an input coupling mirror attached on a PZT. The small (blue) spheres represent singly trapped atoms in lattice sites. The linear polarization of the electric field are indicated by (red) arrows.

lattice cavity with an efficiency of 80%, resulting in $P_{\text{cav}} = 2$ W. A piezoelectric transducer (PZT) attached on the input coupler controlled the lattice cavity length to be resonant with the lattice laser.

The cavity consisted of concave mirrors with different curvatures that were assembled on a stainless steel block set inside the vacuum chamber. The lattice beams were aligned so that all six beams overlap in the 3D trapping region before evacuation. A linearly polarized ($\parallel \mathbf{e}_y$) lattice laser was coupled as shown in Fig. 1. The 3D lattice trap was composed of three linearly polarized electric fields oscillating in phase; two of them ($\mathbf{E}_2, \mathbf{E}_3 \parallel \mathbf{e}_x$) had the same polarization vector and the other ($\mathbf{E}_1 \parallel \mathbf{e}_y$) was perpendicular to the first two, where \mathbf{e}_j is the unit vector in the j direction. The total electric field \mathbf{E}_L , therefore, had linear polarization in the xy plane with the polarization vector spatially varied in the plane. The radii of the lattice beams corresponding to $\mathbf{E}_1, \mathbf{E}_2$, and \mathbf{E}_3 were $(w_1, w_2, w_3) = (260 \mu\text{m}, 260 \mu\text{m}, 130 \mu\text{m})$ at the intersection. The atoms were efficiently loaded into the lattice, as the trap volume was comparable to that of the atomic cloud magneto-optically trapped on the 1S_0 - 3P_1 intercombination transition [40].

Near the center of the 3D lattice, the Stark potential is given by

$$U(x, y, z) = -\frac{1}{2}\alpha_{E1}|\mathbf{E}_L|^2 = U_0(\mathbf{e}_y \cos kx + \mathbf{e}_x \cos ky + 2\mathbf{e}_x \cos kz)^2, \quad (1)$$

where $k = \lambda_L/2\pi$ is the wave number of the lattice laser, $U_0 = -\frac{\alpha_{E1}}{2\epsilon_0 c} \frac{8P_{\text{cav}}}{\pi w^2}$ is the potential depth of a 1D optical lattice with its $1/e^2$ beam radius of $w = w_1 = w_2 = 2w_3$, α_{E1} is the

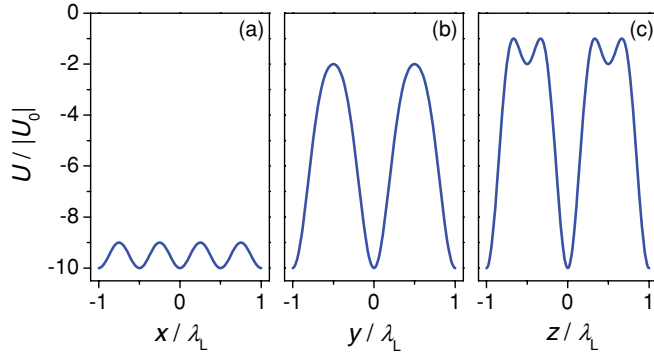


FIG. 2. (Color online) Lattice potential along the (a) x axis, (b) y axis, and (c) z axis in the unit of normalized potential depth $|U_0|$, see text.

electric dipole polarizability of atoms at the magic wavelength λ_L , ϵ_0 is vacuum permittivity, and c is the speed of light. Figures 2(a)–2(c) show the lattice potentials along the x , y , and z axes, respectively. The potential along the z axis, on which we introduce the clock laser, is given by

$$U(0, 0, z) = 2U_0(\cos 2kz + 2 \cos kz + 2). \quad (2)$$

This double periodic structure is due to the interference of the electric fields \mathbf{E}_2 and \mathbf{E}_3 , which are in phase at the positions of $z = n\lambda_L$ and are out of phase at $z = (n + \frac{1}{2})\lambda_L$ with n an integer. By Taylor expanding $U(0, 0, z)$ for $|z| \ll \lambda_L$, the trap frequency is given by $\omega_z = k\sqrt{\frac{12|U_0|}{m}}$.

The actual trap depth was estimated from the motional-sideband frequency, which was measured to be $\omega_z/2\pi = 60(10)$ kHz by the clock laser propagating along the z direction. This suggested the maximum light shift to be $10|U_0| = 130(40)E_r$, corresponding to the lattice peak intensity of $I_0 = 33(10)$ kW/cm², where $E_r = (h/\lambda_L)^2/2m$ is the recoil energy of an atom by the lattice photon. This peak intensity, however, was nearly half of the peak intensity expected for $P_{\text{cav}} = 2$ W in Eq. (1), possibly due to the imperfect overlap of the three standing waves forming the lattice.

Assuming the peak intensity to be $I_0 = 33(10)$ kW/cm², the lattice potential depth along the x direction created by \mathbf{E}_1 [see Fig. 2(a)] was $13 E_r$, which supports only two vibrational bands of $n_x = 0, 1$. Moreover, as a result of this relatively weak confinement, the energy bandwidth (Bloch bandwidth) of the $n_x = 0$ band is calculated to be as large as $\nu_B(0) = 140$ Hz unless external acceleration is applied. In the experimental setup shown in Fig. 1, the Bloch bandwidth was significantly reduced by the gravitational potential difference [41] between adjacent sites $h\nu_g = mg(\lambda_L/2) \cos \varphi \approx h \times 800$ Hz, where $\varphi = 24^\circ$ denoted the angle between gravity and the x axis and h the Planck constant. For atoms occupying the $n_x = 1$ state, as the Bloch bandwidth (in the absence of acceleration) of $\nu_B(1) = 2.6$ kHz well-exceeded ν_g , the gravitational acceleration is not enough to suppress tunneling. We therefore depleted these atoms by temporarily reducing the lattice depth by 50% as described in Sec. III A. Note that the lattice potentials formed in both the y and z directions by the electric fields of \mathbf{E}_2 and \mathbf{E}_3 were as deep as $130E_r$, therefore, the site-to-site atom tunneling rate was negligible regardless of the gravitational potential difference.

This temporary reduction of the lattice potential depth mentioned earlier also allowed removing atoms trapped in the 1D and 2D lattice region, which were formed outside the central 3D lattice. Because of the gravitational potential barrier, the radial confinement of each 1D lattice provided by \mathbf{E}_1 , \mathbf{E}_2 , and \mathbf{E}_3 becomes too weak to support atoms against gravity, which are $mg \sin \varphi$, $mg \cos \varphi$, and mg , respectively. Even after the process, atoms in the two-dimensional (2D) lattice formed by \mathbf{E}_1 and \mathbf{E}_2 may remain trapped. The clock signal from these atoms may well be neglected, as the clock spectrum observed for these atoms will be 10^4 times weaker than that of atoms in the 3D lattice because of the Doppler broadening as large as 100 kHz [42] due to the lack of the Lamb-Dicke confinement.

III. SPECTROSCOPY ON THE CLOCK TRANSITION

A. Preparation of a 3D lattice with single atom occupation

Ultracold ⁸⁸Sr atoms were prepared by two-stage magneto-optical cooling and trapping on the $^1S_0 \rightarrow ^1P_1$ transition at 461 nm and afterward on the $^1S_0 \rightarrow ^3P_1$ intercombination transition at 689 nm [40]. About 10^8 atoms at a few mK were trapped in the first cooling stage in 200 ms. They were cooled down to a few μ K and magneto-optically trapped in the second cooling stage of 150 ms. To efficiently transfer atoms into the lattice, a bias magnetic field was applied to fine-tune the position of the magneto-optically trapped atoms. After transferring atoms into the 3D lattice, the photoassociation was induced by the cooling laser [43,44] near resonant to the $^1S_0 \rightarrow ^3P_1$ transition to remove lattice sites that had more than one atom. The effect was inferred by the fluorescence decay of the trapped atoms: An initial nonexponential atom decay indicated the two-body atom loss, which approached an exponential decay after 20 ms of irradiation.

After turning off the photoassociation laser, the lattice laser intensity I_0 was decreased to about $I_0/2$ in 20 ms to prepare a pure 3D lattice by removing atoms trapped in both the 1D and 2D regions and in the $n_x \geq 1$ state as described previously. After 10 ms, we increased the intensity back to the initial intensity of I_0 in 20 ms. In this way, we prepared a singly-occupied 3D lattice with typically 10^5 bosonic ⁸⁸Sr atoms. The shot-to-shot atom number fluctuation was less than 20%. The storage time of atoms in the lattice was about 500 ms, limited mainly by rest-gas collisions at a pressure of 1×10^{-8} Torr. The atomic temperature in the lattice was estimated from the velocity distribution of atoms released from the lattice by using a time-of-flight method. The temperature in the vertical direction in the lattice was 2μ K, whereas that of the horizontal direction was 4μ K. This anisotropy may be attributed to the different trap frequencies ω_x and ω_z in the x and z directions, as the atoms nearly occupied the vibrational ground state, especially in the x direction.

B. Magnetically induced clock transition

An external magnetic field was applied to introduce a transition dipole moment on the $^1S_0 \rightarrow ^3P_0$ clock transition of ⁸⁸Sr by mixing the 3P_0 state with the 3P_1 state that has a transition moment to the 1S_0 state. The Rabi frequency for the

clock transition is given by [28]

$$\Omega_R = \alpha \sqrt{I_c} (\mathbf{B}_m \cdot \mathbf{E}_c / |\mathbf{E}_c|), \quad (3)$$

where \mathbf{B}_m is the mixing magnetic field in T, I_c is the clock laser intensity in mW/cm^2 , \mathbf{E}_c is the electric field vector of a linearly polarized clock laser, and $\alpha = 198 \text{ Hz}/(\text{T}\sqrt{\text{mW}/\text{cm}^2})$ [28] is the coupling coefficient for Sr. The second-order Zeeman shift is given by

$$\Delta_B = \beta |\mathbf{B}_m|^2, \quad (4)$$

with $\beta = -23.3 \text{ MHz}/\text{T}^2$ and the clock light shift $\Delta_L = \kappa I_c$ with $\kappa = -18 \text{ mHz}/(\text{mW}/\text{cm}^2)$.

In the experiment, the mixing magnetic field \mathbf{B}_m was set in the same xy plane as the lattice field \mathbf{E}_L to minimize the mutual coupling given by Eq. (8) as discussed later, which gives rise to lattice polarization effects [30]. The electric field \mathbf{E}_c of the clock laser was set parallel to the mixing magnetic field \mathbf{B}_m to maximize the Rabi frequency $\Omega_R = \alpha \sqrt{I_c} |\mathbf{B}_m|$. Typically, a magnetic field of $|\mathbf{B}_m| = 2.34 \text{ mT}$ and a clock laser intensity of $I_c = 400 \text{ mW}/\text{cm}^2$ were applied to achieve a Rabi frequency of 9 Hz on the clock transition. These parameters, in turn, resulted in the second-order Zeeman shift of $\Delta_B = -129 \text{ Hz}$ and the clock light shift of $\Delta_L = -7.5 \text{ Hz}$. The $1/e^2$ beam radius of the clock laser was $300 \mu\text{m}$, which was about three times larger than the size of the atomic clouds in the 3D lattice. The relevant intensity inhomogeneity over atoms in the 3D lattice was estimated to be less than 20%.

C. Clock laser

A schematic of the clock laser operating at 698 nm is shown in Fig. 3 [13]. An external cavity diode laser (ECDL) was prestabilized to a medium-finesse cavity made of an Invar spacer. The laser was further stabilized to a high-finesse ($\mathcal{F} \approx 4.3 \times 10^5$) reference cavity consisting of silica mirrors optically contacted on an ultra-low-expansion (ULE) glass spacer. The ULE cavity was vertically mounted [45] inside a vacuum chamber, which was set on a vibration isolation table (150BM-1, Minus-K) placed in a soundproof box. This master laser with a linewidth less than 10 Hz was coupled

to a 30-m-long polarization-maintaining (PM) single-mode optical fiber in which a fiber noise-cancellation system [46] was installed.

Two antireflection-coated diode laser (HL6738MG, Hitachi) were injection locked to the delivered light to amplify the power up to 8 mW, which were then used to interrogate the bosonic 3D and fermionic 1D lattice clocks [13]. Diffraction gratings with 2400 lines/mm were inserted after the amplifier diode laser (DL) to remove the amplified spontaneous emission (ASE) component. The clock lasers were sent to the lattice chambers by optical fibers. The laser intensities were monitored by photodiodes (PD) and acousto-optic modulators (AOM) 1 and 2 were used to stabilize the intensity within 0.5%, keeping the Rabi frequency constant. AOM-3 and 4 were used to generate the π -pulse for the clock excitation.

D. Laser stabilization to the clock transition

Figure 4(a) shows the timing operation chart for the 3D lattice clock. The atomic transitions corresponding to the respective laser wavelengths are depicted in Fig. 5. Laser cooled ^{88}Sr atoms were loaded into the lattice by $t = 350 \text{ ms}$. After turning off the cooling lasers, the mixing magnetic field was increased up to $|\mathbf{B}_m| = 2.34 \text{ mT}$. We then excited the atoms by the clock laser with a pulse duration of $\tau_c = 60 \text{ ms}$. A laser near resonant to the $^1S_0 - ^1P_1$ transition was applied during $610 \text{ ms} < t < 620 \text{ ms}$ to measure the clock excitation. The fluorescence intensity I_S was measured by a photomultiplier tube (PMT) to evaluate the number of atoms N_S remaining unexcited in the 1S_0 ground state. The fluorescence typically decayed in about 1 ms, which indicated the atoms in the ground state were heated out of the lattice by this measurement. Afterward an optical pumping laser resonant to the $5s5p^3P_0 - 5s6s^3S_1$ transition at 679 nm was applied at $t = 630 \text{ ms}$ to transfer the atoms in the 3P_0 excited state to the 1S_0 ground state via the 3P_1 state. After the population transfer, we similarly measured the laser-induced fluorescence intensity I_P on the $^1S_0 - ^1P_1$ transition to deduce the number of atoms N_P in the 3P_0 state. Given a population transfer efficiency of ξ from the 3P_0 state to the 1S_0 ground

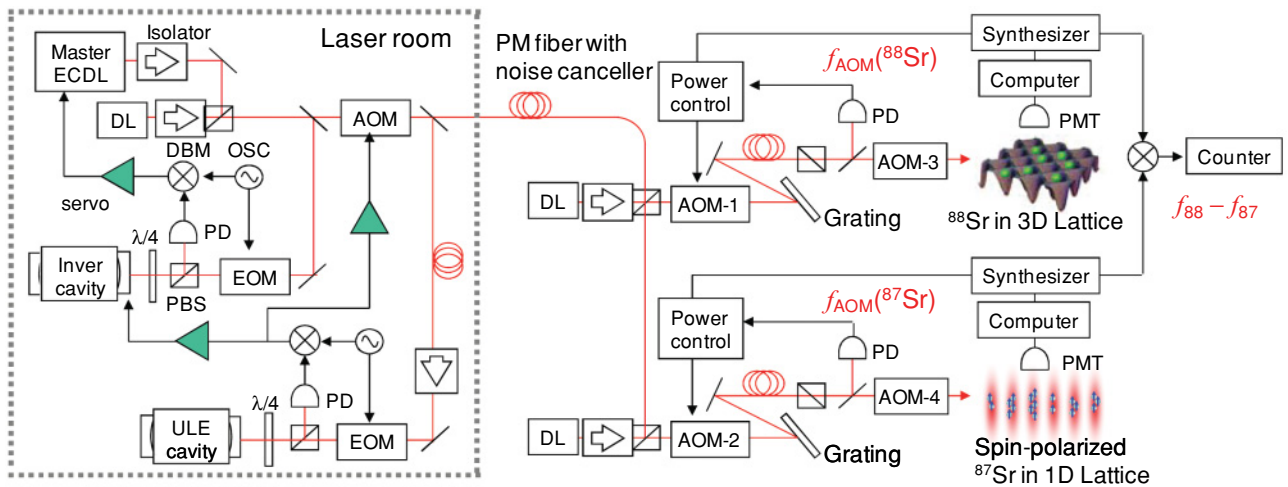


FIG. 3. (Color online) Experimental setup: The clock lasers and the beat-note measurement between bosonic 3D and fermionic 1D lattice clocks. Polarizing beam splitter (PBS); radio frequency oscillator (OSC); double balanced mixer (DBM); and diode laser (DL).

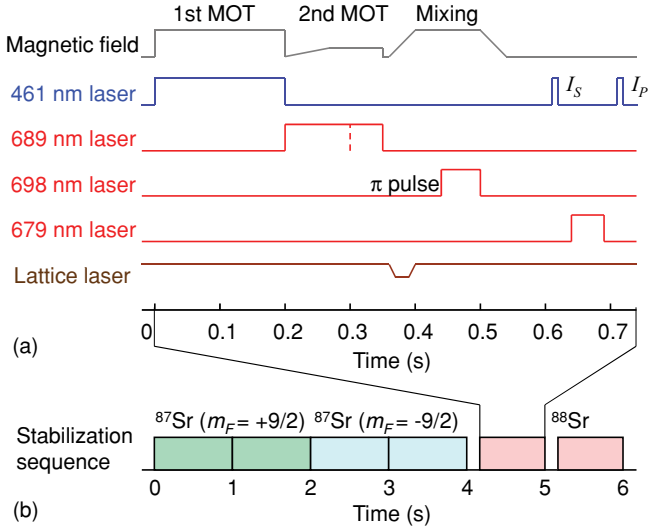


FIG. 4. (Color online) Timing chart for (a) the 3D optical lattice clock with ^{88}Sr and (b) the comparison of ^{87}Sr and ^{88}Sr clocks.

state, the excited atom fraction κ was calculated as

$$\kappa = \frac{N_P}{N_S + N_P} = \frac{I_P}{\xi I_S + I_P}. \quad (5)$$

We experimentally determined the population transfer efficiency to be $\xi = 0.3$, which was in reasonable agreement with the calculated efficiency of $3/8$ given by the branching ratio of the 3S_1 state decaying into either the 3P_1 or the 3P_2 states.

Figure 6(a) shows a typical spectrum of the clock transition excited by a 60-ms-long π pulse of the clock laser with Rabi frequency $\Omega_R/2\pi = 9$ Hz. We observed a nearly Fourier-limited 13-Hz-wide spectrum with maximum excitation of $\kappa \approx 0.8$. Figure 6(b) shows the corresponding Rabi oscillation. The reduced contrast is caused by the inhomogeneity of the

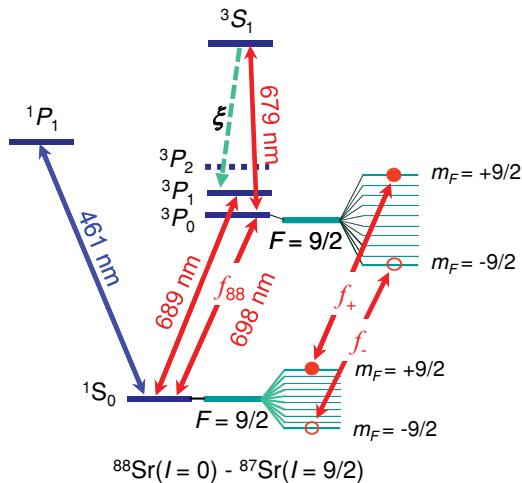


FIG. 5. (Color online) Energy level diagram of bosonic ^{88}Sr and fermionic ^{87}Sr isotopes with the clock frequencies of f_{88} and $f_{87} = (f_+ + f_-)/2$, respectively. The fermionic isotope has nuclear spin of $I = 9/2$, resulting in the hyperfine structure and related Zeeman substates.

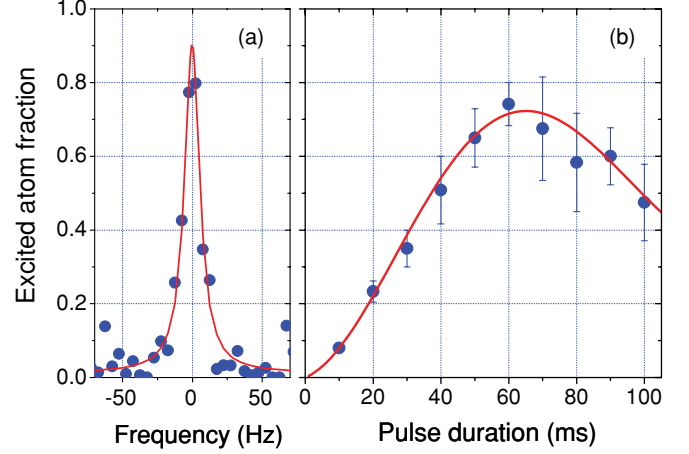


FIG. 6. (Color online) (a) A typical spectrum of the clock transition of ^{88}Sr in the 3D optical lattice. (b) The Rabi oscillation on the clock transition. In both measurements the maximum excitation fraction was nearly 0.8.

Rabi frequency among atoms, attributed to the spatial intensity variation of the clock laser and the thermal vibrational state occupation in the lattice potentials.

The clock laser was frequency stabilized to the center of the excitation spectrum with a full width at half maximum (FWHM) linewidth of $\gamma \approx 13$ Hz as shown in Fig. 6(a). At $t = t_n$, the stabilized clock laser frequency was given by $f_c(t_n) = f_{\text{ULE}}(t_n) + f_{\text{err}}(t_n)$, where $f_{\text{ULE}}(t_n)$ was the clock laser frequency stabilized to the ULE cavity and $f_{\text{err}}(t_n)$ the correction frequency fed by computer control. By alternately setting the frequency of AOM-1 or 2 in Fig. 3 as $f_{\text{AOM}}(t_n) = f_{\text{err}}(t_n) \pm \gamma/2$, the corresponding excitation probability $\kappa_{\pm}(t_n)$ was measured to derive the error signal $e(t_n) = \kappa_+(t_n) - \kappa_-(t_n)$ used for the stabilization. Using the error signal, the AOM frequency at $t = t_{n+1}$ was given by

$$f_{\text{err}}(t_{n+1}) = f_{\text{err}}(t_n) + g_I \frac{\gamma}{2} e(t_n), \quad (6)$$

where g_I is the feedback gain of the integral control loop [13,47]. In this first-order integral feedback, the feedback gain is optimized at $g_I = 1/\kappa_0$ for the peak excitation probability of κ_0 . In addition, we feed forward a linear frequency chirp to compensate for the ≈ 1 Hz/s drift of the ULE cavity.

IV. FREQUENCY COMPARISON BETWEEN TWO OPTICAL LATTICE CLOCKS

A. 1D lattice clock with spin-polarized fermionic ^{87}Sr as a reference

We used the optical lattice clock with spin-polarized ^{87}Sr atoms as a reference to evaluate the uncertainties and corrections of the bosonic 3D optical lattice clock. Figure 3 shows a schematic diagram of the experiment. The experimental details for the spin-polarized ^{87}Sr clock are described elsewhere [13,26,31]. Roughly 10^4 fermionic ^{87}Sr atoms at a temperature of $2 \mu\text{K}$ were loaded into a $10\text{-}\mu\text{K}$ -deep 1D lattice. The atoms were spin polarized by a circularly polarized optical-pumping laser operating on the $^1S_0(F = 9/2) \rightarrow ^3P_1(F = 9/2)$ transition at 689 nm in a presence of a weak bias magnetic field

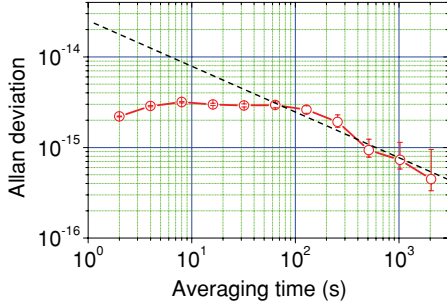


FIG. 7. (Color online) Allan deviation for the beat note $\delta = f_{88} - f_{87}$ of the two lattice clocks operated with different isotopes. The dashed line shows the asymptotic stability of $\sigma_y(\tau) = 2.3 \times 10^{-14}/\sqrt{\tau}$.

$|\mathbf{B}_0| \approx 5 \mu\text{T}$ that defined the quantization axis. The clock frequency f_{87} for ^{87}Sr was detuned with respect to f_{88} of ^{88}Sr by the isotope shift of about 62 MHz. The bias magnetic field was increased to $|\mathbf{B}_0| = 0.182 \text{ mT}$ to resolve adjacent Zeeman components in the $^1S_0(F=9/2)^{-3}P_0(F=9/2)$ clock transition. A 60-ms-long π -pulse was applied to observe a 13-Hz-wide clock spectrum on the $^1S_0(F=9/2, m_F = \pm 9/2)^{-3}P_0(F=9/2, m_F = \pm 9/2)$ transitions with transition frequencies f_{\pm} , respectively (see Fig. 5). The average frequency of two transitions $f_{87} = (f_+ + f_-)/2$ was equivalent to the clock transition frequency of ^{87}Sr free from the first order Zeeman shift and the vector light shift [13].

Figure 4(b) shows six successive interrogations that were used to servo control the clock laser frequencies f_+ , f_- , and f_{88} with a cycle time 6 s. The Allan deviation of the beat frequency $\delta = f_{88} - f_{87}$ was calculated as shown in Fig. 7 using the data measured over 10,000 s to evaluate the stability of optical lattice clocks. For an average time $\tau > 100 \text{ s}$, the Allan deviation decreased with $\sigma_y(\tau) = 2.3 \times 10^{-14}/\sqrt{\tau}$ and reached 5×10^{-16} at an average time $\tau = 2000 \text{ s}$. The measured stability was 10^2 times worse than that of the quantum projection noise (QPN) limited stability $\sigma_y(\tau) = 1 \times 10^{-16}/\sqrt{\tau}$ expected for the 13-Hz-wide clock spectra with 10^5 atoms, which may be explained by the Dick effect [48] as follows.

B. THE DICK EFFECT

In the frequency stabilization method described previously, the interrogation of atomic transitions and frequency steering processes are discontinuous and periodic. Such a stabilization scheme degrades the stability of microwave clocks [48,49] and the optical clocks [50] by the so-called Dick effect. As described in Sec. III D, the error signal $e(t_n)$ was determined by the clock laser interacting with atoms during the two pulsed Rabi interrogating periods each lasting $T_i = 60 \text{ ms}$, which is a small fraction of a whole cycle time of $T_{\text{cyc}} = 6 \text{ s}$. Afterward the clock frequency $f_c \approx 429 \text{ THz}$ was controlled.

This situation is equivalent to measuring a laser frequency by a counter with its gate time T_i at every $T_{\text{cyc}} (> T_i)$. Frequency fluctuations higher than the Nyquist frequency $f_N = 1/(2T_{\text{cyc}})$ disturb the measurement by aliasing, as the frequency noise at around the cycle frequency $1/T_{\text{cyc}}$ and its harmonics higher than the Nyquist frequency f_N are down-converted into low

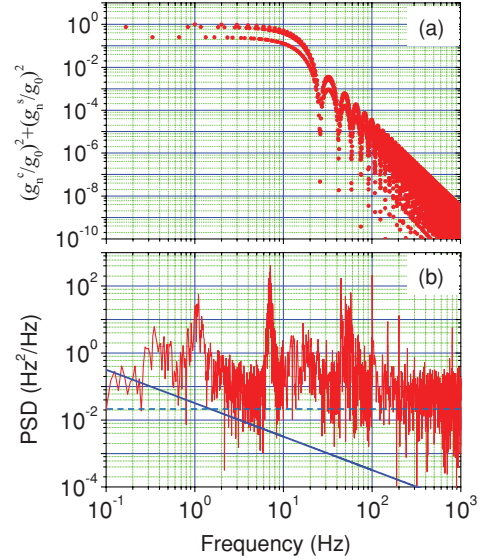


FIG. 8. (Color online) (a) $(g_n^c/g_0)^2 + (g_n^s/g_0)^2$ as a function of frequency. (b) The power spectrum density (PSD) $f_c^2 S_y^f(f)$ of the clock laser used in the experiment (red line). The (blue) solid and dashed lines indicate the thermal noise and residual white noise corresponding to $f_c^2 S_y^f(f) = 0.032/f + 0.02$.

frequencies $f \ll 1/T_{\text{cyc}}$. This aliasing noise, mixed in with the error signal in a feedback loop, causes a long-term white frequency noise in the stabilized laser [49]. The Allan variance $\sigma_y^2(\tau)$ in the presence of the aliasing noise is given by

$$\sigma_y^2(\tau) = \frac{1}{\tau} \sum_{n=1}^{\infty} \left[\left(\frac{g_n^c}{g_0} \right)^2 + \left(\frac{g_n^s}{g_0} \right)^2 \right] S_y^f \left(\frac{n}{T_{\text{cyc}}} \right), \quad (7)$$

where $S_y^f(n/T_{\text{cyc}})$ is the power spectral density of the clock laser sampled at frequencies $f = n/T_{\text{cyc}}$, g_0 is the mean value of the sensitivity function $g(t)$ [49] in a cycle, and g_n^c and g_n^s are the Fourier coefficients of $g(t)$ for the $\sin(n/T_{\text{cyc}})$ and $\cos(n/T_{\text{cyc}})$ components.

Figure 8(a) shows $(g_n^c/g_0)^2 + (g_n^s/g_0)^2$ as a function of $f = n/T_{\text{cyc}}$ calculated for our experimental sequence time of $T_i = 60 \text{ ms}$ and $T_{\text{cyc}} = 6 \text{ s}$. As $(g_n^c/g_0)^2 + (g_n^s/g_0)^2$ rapidly decreases as f^{-4} for frequencies higher than $f_i = 1/T_i$, we truncated the summation in Eq. (7) at 1 kHz. Figure 8(b) shows the power spectrum density $f_c^2 S_y^f(f)$ of the clock laser, which was measured by referencing an independently prepared ULE cavity with similar stability as the other. As a reference, the thermal noise of the reference cavity [51] and the typical white-noise level in the measurement as reported in Ref. [52] are indicated by the solid and dashed lines, respectively, in Fig. 8(b). Applying $S_y^f(f)$ measured for our clock laser in Eq. (7), we obtained $\sigma_y(\tau) = 3.4 \times 10^{-14}/\sqrt{\tau}$ as the Dick limit, which was comparable to the experimentally measured stability of $\sigma_y(\tau) = 2.3 \times 10^{-14}/\sqrt{\tau}$.

The Dick-effect-limited stabilities at $\tau = 1 \text{ s}$ for various experimental conditions were calculated using the power spectrum density measured for our clock laser. Figure 9(a) shows the stability as a function of the interrogating time T_i for the fixed cycle time of $T_{\text{cyc}} = 2 \text{ s}$, which can be experimentally realized by simultaneously operating the 3D and 1D clocks.

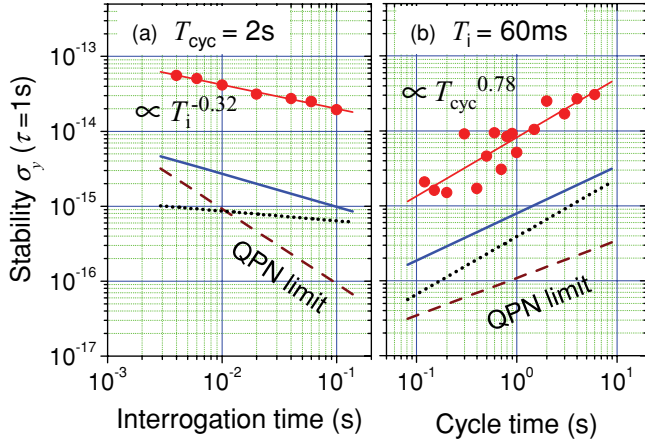


FIG. 9. (Color online) The Dick limited stabilities at $\tau = 1$ s are shown by (red) circles, which are fitted by (red) solid lines. They were calculated as functions of (a) the interrogating time T_i with $T_{\text{cyc}} = 2$ s and (b) the cycle time T_{cyc} with $T_i = 60$ ms, assuming the laser noise spectrum used in the experiment. The (black) dotted lines assumed a clock laser operated at the thermal noise limit in addition to the photon shot noise. The (blue) solid lines further assumed a white noise floor of technical origin (see text). The (brown) dashed lines indicate the QPN limit for 10^5 atoms.

Alternatively, for a fixed interrogating time of $T_i = 60$ ms, the cycle time T_{cyc} dependence of the stability was calculated in Fig. 9(b). The stability is roughly proportional to $T_{\text{cyc}}^{0.78}/T_i^{0.32}$, suggesting that the reduction of the cycle time T_{cyc} is crucial in achieving the higher stability.

In the present experiment, the cycle time of $T_{\text{cyc}} = 6$ s is given by the experimental sequence time while the interrogating time $T_i = 60$ ms is limited by the clock laser linewidth, both of which can be further improved in the future. By optimizing the laser-cooling process and by operating the two lattice clocks simultaneously, T_{cyc} can be reduced to less than 1 s, improving the Dick limited stability up to $\sigma_y(\tau) = 8 \times 10^{-15}/\sqrt{\tau}$. A minimally destructive measurement [53] of atoms in the lattice trap, which allows using the same atomic sample without reloading atoms for each measurement as in the case of ion clocks [5], may allow further reduction of the cycle time down to $T_{\text{cyc}} \approx 2T_i$.

In future experiments, the power spectrum density of the clock laser will be limited mostly by the thermal noise [51] of $f_c^2 S_y^f(f) = 0.032/f$ (Hz^2/Hz) as shown by the (blue) solid line in Fig. 8(b), where we assumed a 75-mm-long reference cavity consisted of the 25.4-mm-diameter ULE spacer with 200 μm beam radius on the fused silica mirror. The corresponding Dick-effect-limited stabilities are shown by dotted lines in Fig. 9, where the shot-noise limit given by the 10 μW of laser power is assumed. In practice, however, the stabilities may be limited by a white-noise floor $\approx 0.02(\text{Hz}^2/\text{Hz})$ of technical origin [52] as indicated in Fig. 8(b). The resultant Dick-effect-limited stability is calculated to be $\sigma_y^{\text{Dick}}(1\text{s}) = 2.3 \times 10^{-16} \times T_{\text{cyc}}^{0.63}/T_i^{0.45}$ as indicated by the (blue) solid lines in Fig. 9. The dashed lines show the QPN limited stability expected for the $N = 10^5$ atoms observed with the Fourier limited linewidth $\Delta f = 0.89/T_i$ in each cycle time T_{cyc} , which is given by $\sigma_y^{\text{QPN}}(1\text{s}) = 6.5 \times 10^{-18} \times T_{\text{cyc}}^{1/2}/T_i$. In

the limiting case $T_{\text{cyc}} \approx 2T_i$ (by reducing the cycle time T_{cyc}), the $\sigma_y^{\text{Dick}}(1\text{s})$ improves, however, the QPN limited stability $\sigma_y^{\text{QPN}}(1\text{s}) = 1.3 \times 10^{-17} \times T_{\text{cyc}}^{-1/2}$ deteriorates and becomes closer to $\sigma_y^{\text{Dick}}(1\text{s})$. We anticipate that a clock stability $\sigma_y(\tau) = 2 \times 10^{-16}/\sqrt{\tau}$ will be feasible assuming $T_{\text{cyc}} \approx 2T_i = 0.1$ s for $N = 10^5$ atoms.

V. CORRECTIONS AND UNCERTAINTIES FOR MAGNETICALLY INDUCED CLOCK

Table I summarizes the corrections and uncertainties for the 3D clock with ^{88}Sr atoms. In a magnetically induced bosonic clock with ^{88}Sr atoms, the second-order Zeeman shift dominates the clock shift corrections. Using a weighted average for ten data sets [31] measured over four months, we determined the isotope shift to be $f_{88} - f_{87} = 62, 188, 138.5(1.3)$ Hz.

A. Second-order Zeeman shift

Three pairs of Helmholtz coils, $\mathcal{H}1$, $\mathcal{H}2$, and $\mathcal{H}3$ with current j_1 , j_2 , and j_3 were used to apply magnetic field onto the interrogated atoms. $\mathcal{H}1$ consisted of two coils with radii of 98 mm separated by 98 mm to produce a spatially uniform mixing field $\mathbf{B}_m(\parallel \mathbf{E}_c)$. The spatial inhomogeneity of \mathbf{B}_m was estimated to be less than 10 nT across the lattice region. The axes of $\mathcal{H}2$ and $\mathcal{H}3$ were set orthogonal to each other and perpendicular to $\mathcal{H}1$. $\mathcal{H}2$ and $\mathcal{H}3$ control the transverse magnetic field \mathbf{B}_\perp . The total magnetic field in the lattice region was given by $\mathbf{B} = \mathbf{B}_m + \mathbf{B}_\perp$, including the ambient magnetic fields such as Earth's magnetic field and those generated by nearby apparatuses.

In magnetically induced spectroscopy, j_2 and j_3 were adjusted so that the transverse magnetic field \mathbf{B}_\perp is zero and j_1 was set to give $|\mathbf{B}_m| = 2.34$ mT. This mixing field gave the second-order Zeeman shift of $\Delta_B = -128.6(3)$ Hz according to Eq. (4). The uncertainty was partly due to the inhomogeneity of the ambient magnetic field of about 1 μT across the lattice region, which was caused by an ion pump and an optical isolator placed several cm away from the lattice region.

The total magnetic field \mathbf{B} was measured by the Zeeman shift of the transition frequency $f_{\pm 1}$ on the $^1S_0 - ^3P_1(m_J = \pm 1)$ transition at 689 nm with the linewidth of 7.5 kHz. To suppress the Doppler shifts in the measurement ^{88}Sr atoms were trapped in the 3D lattice operated at $\lambda_L = 813.428$ nm. Because of the differential light shift on the relevant transition [42], typically 70-kHz-wide spectra were observed, which allowed

TABLE I. Uncertainty budgets for the ^{88}Sr lattice clock.

Contributor	Correction (Hz)	Uncertainty (Hz)
2nd-order Zeeman shift	128.61	0.31
Clock light shift	7.48	0.36
Lattice light shift		
scalar	-0.17	1.07
polarization effects	0	0.012
fourth-order	-0.07	0.15
Blackbody shift	2.4	0.2
Collisional shift	-0.034	0.3
Systematic total	138.22	1.23

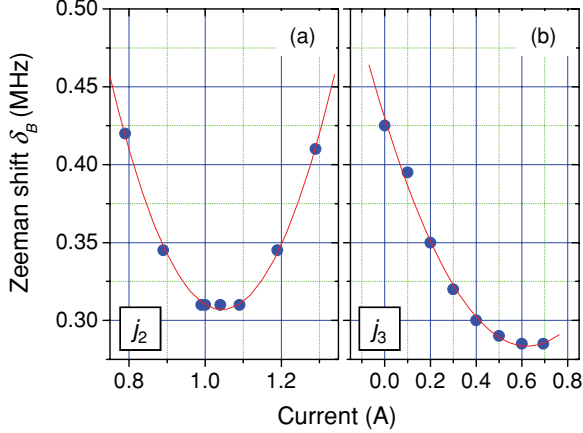


FIG. 10. (Color online) The (first-order) differential Zeeman shift $\delta_B = (f_{+1} - f_{-1})/2$ as a function of the current (a) j_2 and (b) j_3 in the presence of $|\mathbf{B}_m| = 0.015$ mT.

determining the center frequency within 6 kHz equivalent to the magnetic field uncertainty of $0.3 \mu\text{T}$. Note that the differential Zeeman shift $\delta_B = (f_{+1} - f_{-1})/2$ can be free from the differential light shift of the lattice as long as the local polarization in the lattice sites are linear. Therefore, δ_B served as a sensitive probe to determine the magnetic field as $|\mathbf{B}| = \delta_B/21.0033(5)$ mT/MHz, where $g_J(^3P_1) = 1.50065(4)$ [54] was used for the g factor in the 3P_1 state.

To null the transverse magnetic field $|\mathbf{B}_\perp|$, we tuned j_2 and j_3 to minimize δ_B as shown in Fig. 10(a) and 10(b) in the presence of $|\mathbf{B}_m| \approx 15 \mu\text{T}$ generated by j_1 . For $|\mathbf{B}_\perp| \ll |\mathbf{B}_m|$, the Zeeman shift varied parabolically as $|\mathbf{B}| \approx |\mathbf{B}_m| + |\mathbf{B}_\perp|^2/(2|\mathbf{B}_m|)$. $|\mathbf{B}_\perp| < 3 \mu\text{T}$ was realized for $j_2 = 1044(2)$ mA and $j_3 = 620(30)$ mA. Under this condition, the Zeeman shift was measured to be $\delta_B = 49.177(14)$ MHz for $j_1 = 27.550(8)$ A, which gave the bias field of $|\mathbf{B}_m| = 2.34$ mT used in the state mixing. The fluctuation of j_1 during a few hours of the experiment was about 0.03% due to the current fluctuation of the power supply, corresponding to $0.7 \mu\text{T}$ uncertainty in $|\mathbf{B}_m|$, resulting in 80 mHz of uncertainty in Δ_B .

We used the 1D lattice clock with ^{87}Sr with frequency f_{87} as an anchor to investigate systematic corrections of f_{88} , as it is significantly immune to systematic clock shifts [31]. Figure 11 shows the beat note $\delta = f_{88} - f_{87}$ measured as a function of $|\delta_B|^2 (\propto |\mathbf{B}_m|^2)$ with the clock laser intensity of $I_c = 400$ mW/cm 2 . The beat note δ was determined by operating both clocks for about 2000 s, yielding an Allan deviation $\sigma_y \approx 2 \times 10^{-15}$ for an averaging time of 200 s (see Fig. 7). We conservatively took this uncertainty of a few Hz as that for the beat-note measurements. By measuring δ for five different parameters of $|\mathbf{B}_m|$ and extrapolating them to zero we determined the second-order Zeeman shift of the ^{88}Sr based clock (see Table I).

B. Clock light shift

The transition moment of the magnetically induced clock transition of ^{88}Sr with $|\mathbf{B}_m| = 2.34$ mT was about 10^3 times smaller than that of the hyperfine-induced clock transition of ^{87}Sr . As a result, 10^6 times more laser intensity was required to

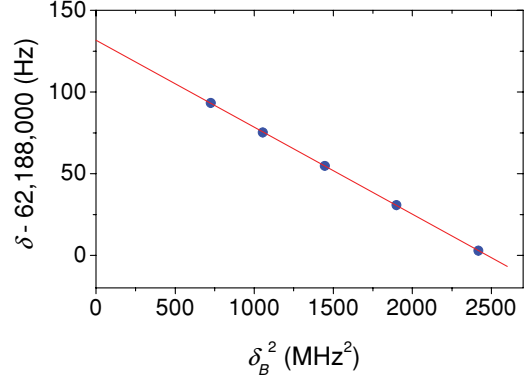


FIG. 11. (Color online). Correction of the second-order Zeeman shift. Beat frequency $\delta = f_{88} - f_{87}$ was plotted as a function of the squared Zeeman shift δ_B^2 . The size of the error bars are well within the filled circles.

excite the clock transition with a similar Rabi frequency as used in ^{87}Sr , causing several Hz of light shift in the clock transition. Figure 12 shows the light shift as a function of the clock laser intensity I_c for the mixing field of $|\mathbf{B}_m| = 2.34$ mT. The light shift due to the clock laser was corrected by measuring the beat note $\delta = f_{88} - f_{87}$ for five different parameters of I_c and extrapolating them to zero.

C. Lattice light shift

1. Scalar and fourth-order light shift

The 3D optical lattice with ^{88}Sr was operated at $\nu_L = c/\lambda_L = 368,554.5(2)$ GHz, the same frequency as ^{87}Sr . However, the magic frequency ν_L depends on the isotope shift of the energy levels. Based on the magic frequency $\nu_L^{(87)} = 368,554.68(18)$ GHz [55] determined for ^{87}Sr , we estimated a correction for ^{88}Sr by taking into account the hyperfine structures as well as the isotope shift of the $5s5p^1P_1$ and $5s6s^3S_1$ states [56,57], which gave about 97% and 50% of light shifts, respectively. The magic frequency for ^{88}Sr was calculated to be $\nu_L^{(88)} = 368,554.58(28)$ GHz, which was about 100 MHz lower than that for ^{87}Sr . Here, the uncertainty was estimated from the contributions of the other states than considered previously.

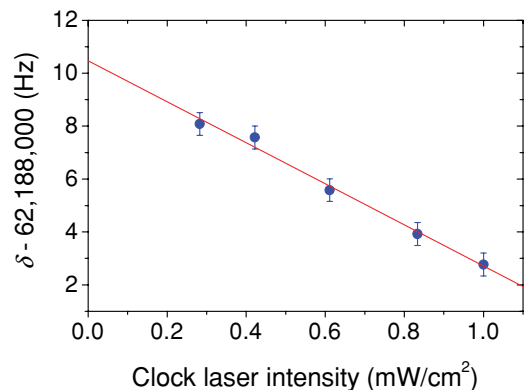


FIG. 12. (Color online) Correction of the clock light shift. Beat frequency $\delta = f_{88} - f_{87}$ was measured as a function of the clock laser intensity I_c to determine $\delta(I_c \rightarrow 0)$.

In evaluating the lattice light shift we took the spatial distribution of the vibrational wave function $\psi(\mathbf{r})$ of atoms into account. The effective lattice laser intensity was calculated to be $\langle I_L \rangle = \int \psi^*(\mathbf{r}) I_L(\mathbf{r}) \psi(\mathbf{r}) d\mathbf{r} = 25(7) \text{ kW/cm}^2$, which was about 25% less than the peak intensity. Here we assumed that atoms were in the $\langle n_x \rangle = 0$, $\langle n_y \rangle \approx 1.5$, and $\langle n_z \rangle \approx 1$ vibrational states in the x , y , and z directions with trap frequencies of $(\omega_x, \omega_y, \omega_z)/2\pi = (25, 43, 60) \text{ kHz}$, respectively, as inferred in the following. In ramping down the lattice laser intensity (see Sec. III. A) only the vibrational ground state ($n_x = 0$) is supported in the x direction, while several levels are supported for n_y and n_z due to the anisotropy of the lattice potential depth as indicated in Fig. 2. Therefore, we assumed thermal distributions for the latter two directions with the atomic temperature of $4 \mu\text{K}$ as measured by the time-of-flight measurements. This effective intensity $\langle I_L \rangle$ led to the scalar light shift of $0.17(1.07) \text{ Hz}$, where relatively large uncertainty was attributed to that of the magic frequency $\nu_L^{(88)}$ as discussed earlier, which should be experimentally determined in future work.

The fourth-order light shift was similarly estimated to be $0.07(15) \text{ Hz}$ based on the squared average of intensity $\langle I_L^2 \rangle = \int \psi^*(\mathbf{r}) I_L^2(\mathbf{r}) \psi(\mathbf{r}) d\mathbf{r}$ by applying the coefficient $(U^2/E_r^2) \times 7(6) \mu\text{Hz}$ measured for ^{87}Sr [58]. While the hyperpolarizability effect is sensitive to the resonances that may be excited by two magic-frequency photons [i.e., $2\nu_L^{(88)}$] the associated transitions $^3P_0-5s7p^1P_1$ and $^3P_0-5s4f^3F_2$ [58] are as far as -31 GHz and $+2.3 \text{ THz}$ detuned from $2\nu_L^{(88)}$. Therefore, the fourth-order light shift measured for ^{87}Sr may well be applied to ^{88}Sr .

2. Lattice polarization effects

The light shift on the 3P_0 state of ^{88}Sr should, in principle, be independent of the light polarization. However, when the state is mixed with the 3P_1 state by the magnetic field \mathbf{B}_m , a fictitious magnetic field \mathbf{B}_f responsible for the elliptically polarized lattice laser [29] will show up as a cross term $\mathbf{B}_m \cdot \mathbf{B}_f$ [30] in the quadratic Zeeman shift for the total magnetic field $\mathbf{B}_m + \mathbf{B}_f$.

The cross term depends on the ellipticity angle ϵ defined by $\mathbf{e}_L = \mathbf{e}_{x'} \cos \epsilon + i \mathbf{e}_{y'} \sin \epsilon$ of the complex unit polarization vector of the lattice electric field \mathbf{E}_L , giving rise to a polarization dependent light shift reminiscent of the vector light shift. Here, $\mathbf{e}_{x'}$ and $\mathbf{e}_{y'}$ are the unit vectors along both the major and minor axes of the polarization ellipse, respectively, thus $i \mathbf{e}_L^* \times \mathbf{e}_L = -\mathbf{e}_{z'} \sin(2\epsilon)$ is perpendicular to the plane of the polarization ellipse of the lattice field. The polarization dependent light shift is described by [30]

$$\begin{aligned} \Delta_B^{(\text{lat})} &= 2\beta\eta I_L (i \mathbf{e}_L^* \times \mathbf{e}_L) \cdot \mathbf{B}_m \\ &= -2\beta\eta I_L |\mathbf{B}_m| \sin(2\epsilon) \cos \theta, \end{aligned} \quad (8)$$

where θ is an angle between $\mathbf{e}_{z'}$ and \mathbf{B}_m , $\eta = 0.893 \text{ mT/(MW/cm}^2)$ is the coupling coefficient for Sr, I_L the laser intensity, and $\beta = -23.3 \text{ MHz/T}^2$ as given previously. Consequently, the lattice polarization effect vanishes by applying a linearly polarized lattice field [$\sin(2\epsilon) = 0$] or by setting the mixing magnetic field in the plane of the polarization ellipse of the lattice field [$\cos \theta = 0$].

In the experiment, the ellipticity of the lattice laser in the cavity was measured to be $\epsilon = 0.05 \text{ rad}$, which may be attributed to the birefringence of the vacuum window inside

the cavity (see Fig. 1). Because of this ellipticity, \mathbf{E}_1 and \mathbf{E}_2 were no longer in the xy plane but had z components. In the lattice sites where \mathbf{E}_1 and \mathbf{E}_2 were in phase, the angle between $\mathbf{e}_{z'}$ and \mathbf{e}_z was estimated to be no greater than $\theta = 0.032 \text{ rad}$. The magnetic field vector \mathbf{B}_m is within 0.01 rad of the xy plane. The uncertainty due to the lattice polarization effect is given in Table I.

Atoms oscillating in the lattice sites see rotating light polarization in the atom-rest frame because of the spatially varying polarization of the lattice electric field. This situation is similar to the 1D molasses with $\sigma^+ - \sigma^-$ laser configuration as discussed in Ref. [59]. We estimate the light shift due to the polarization rotation to be less than 1 nHz . The derivation is described in the Appendix.

D. Collisional shift

In the bosonic 3D lattice clock the residual collisional shift may appear in two cases; (i) some of the lattice sites trap more than one atom or (ii) tunneling of atoms between lattice sites occurs. As described in Sec. III A, we carefully eliminated these effects by inducing photoassociation and by the gravitational potential difference between the adjacent sites, respectively. To confirm the absence of the collisional shifts we investigated the correlation between the clock frequency $\delta(t_n) = f_{88}(t_n) - f_{87}(t_n)$ and the number of interrogated atoms $N_{88}(t_n)$ for the n th interrogation cycle at $t = t_n$ by referencing $f_{87}(t_n)$ of the fermionic 1D clock. The atom number was determined by the fluorescence intensity as $N = N_S + N_P \propto I_S + I_P/\xi$ [see Eq. (5)]. The shot-to-shot atom number fluctuation was less than 20%, while nearly 50% variation was observed over a few 100 s, possibly due to a long-term intensity drift of the cooling lasers on the $^1S_0-^1P_1$ transition. Assuming atomic temperatures and trap confinement to be constant and therefore the trap volume V to be constant, N_{88} can be proportional to the atomic densities N_{88}/V that are related to the collision shifts.

We evaluated the correlation coefficient r_{88} defined by the covariance between $N_{88}(t_n)$ and $\delta(t_n)$ divided by their standard deviations as

$$r_{88} = \frac{\sum_n [N_{88}(t_n) - \bar{N}_{88}] [\delta(t_n) - \bar{\delta}]}{\sqrt{\sum_n [N_{88}(t_n) - \bar{N}_{88}]^2} \sqrt{\sum_n [\delta(t_n) - \bar{\delta}]^2}}, \quad (9)$$

where \bar{N}_{88} and $\bar{\delta}$ are the sample means of $N_{88}(t_n)$ and $\delta(t_n)$. For the ten data sets that were used to derive the isotope shift [31], the coefficients $|r_{88}|$ were less than 0.1, suggesting no noticeable correlation or density shifts. Figure 13 shows the beat note $\delta(t_n)$ as a function of $N_{88}(t_n)$. The linear regression analyses on the ten data sets inferred the correction and uncertainty of the collision shift to be $-0.03(30) \text{ Hz}$.

VI. SUMMARY AND OUTLOOK

We demonstrate a 3D optical lattice clock with bosonic ^{88}Sr and evaluate the stability and uncertainties by referencing the 1D clock with spin-polarized fermionic ^{87}Sr . The Allan deviation achieved is better than 1×10^{-15} for an average time longer than 500 s. The single occupancy 3D lattice is found to be protected from collisional shifts that seriously limited the uncertainty of previous measurements with ^{88}Sr in

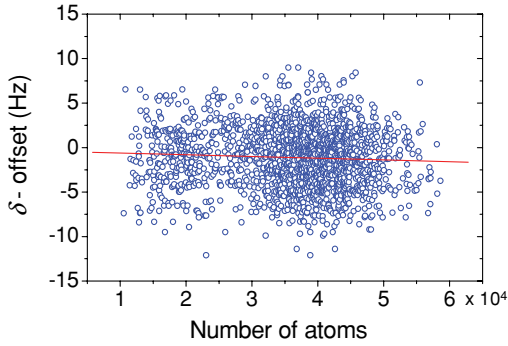


FIG. 13. (Color online) The beat-note frequency $\delta(t_n) = f_{88} - f_{87}$ as a function of interrogated atom number $N_{88}(t_n)$. The (red) solid line shows the linear regression analysis, indicating the collision shift to be $-0.03(30)$ Hz.

a 1D lattice [14]. In addition we show that the uncertainties responsible for the lattice polarization effects can be reduced by properly designing the light polarization of the 3D optical lattice with respect to the mixing electric field.

The magnetically induced clock transition, however, suffers significantly from second-order Zeeman shift Δ_B and the light shift Δ_L of the clock laser, both of which limited our measurement uncertainties to 2×10^{-15} for the ^{88}Sr clock. In future experiments we anticipate that these uncertainties can be reduced to 10 mHz, or 2×10^{-17} fractional uncertainty by controlling $|\mathbf{B}_m| = 2$ mT with 50 nT uncertainty and $I_c = 50$ mW/cm 2 with 1% uncertainty, assuming a Rabi frequency of 3 Hz. The experimental determination of the magic wavelength for ^{88}Sr will further reduce current uncertainties. The present experiment is not optimized for the reduction of the hyperpolarizability effects, it is better to design the lattice to have isotopic potential depth for x , y , and z directions. In addition, atomic multipolar interactions with optical lattices [8], which were not considered here, will be a concern in pursuing the 10^{-18} accuracy.

The 3D lattice geometry may be applied to ^{87}Sr as well, albeit coupling between lattice light polarization and the nuclear spin of $I = 9/2$ may introduce uncertainties in canceling out lattice light shift. Because the electric field polarization is position dependent, a tensor light shift of about 0.7 mHz arises for lattice intensities of 10 kW/cm 2 or a lattice depth of $U = 40E_r$, assuming the tensor shift coefficients $\approx -m_F^2(U/E_r) \times 10^{-6}$ Hz with m_F the magnetic substate. The vector light shift due to ellipticity of the lattice laser [7] may give a principal contribution for the clock line broadening and/or shift of 50 mHz applying the ellipticity and laser intensity measured in this experiment. As discussed in the Appendix, the influence of the polarization rotation for atoms oscillating in the lattice sites will be less than 1 nHz.

As discussed in Sec. III, the current stability is critically limited by the Dick effect as the actual interrogation period was less than one-tenth of the cycle time, most of which was spent cooling and trapping atoms. The application of minimally destructive measurement of the clock state [53,60–62] will allow use of the same atoms repeatedly. The reduced cycle time will improve the stability up to $\sigma(\tau) = 2 \times 10^{-16}/\sqrt{\tau}$, used with the thermal noise limited clock laser. This will allow investigating the clock uncertainties in the 10^{-18} region in an experimentally feasible time scale of a few hours. This may enable us to observe more subtle atomic interactions, such as tunneling assisted collisions, with hitherto unexplored precision, opening up new possibilities such as quantum simulation employing optical lattice clocks as a platform.

ACKNOWLEDGMENTS

This research was supported by the Photon Frontier Network Program of the Ministry of Education, Culture, Sports, Science, and Technology, Japan. The authors would like to thank C. Locke for careful reading of the manuscript and T. Takano for his comments.

APPENDIX: INFLUENCE OF THE ROTATION OF THE LATTICE POLARIZATION

In 3D optical lattices, even if the local light polarization can be made linear, the unit electric field vector $\mathbf{e}_L(\mathbf{r}) = \mathbf{E}_L/|\mathbf{E}_L|$ is necessarily position dependent, which may cause atom-motion-induced light shifts. For simplicity, we consider atoms oscillating along the z direction in the electric field given in Eq. (1) (see Fig. 1), in which the polarization vector $\mathbf{e}_L(\mathbf{r})$ is perpendicular to the direction of atomic motion. For an atom at $\mathbf{r} = (0, 0, z)$, we define the polarization angle $\phi(z) = \cos^{-1}[\mathbf{e}_L(\mathbf{r}) \cdot \mathbf{e}_x] = \cos^{-1} \frac{1+2\cos kz}{\sqrt{1+(1+2\cos kz)^2}}$. The frequency for polarization rotation at $z(t)$ is given by $\nu_r(t) = \frac{1}{2\pi} \frac{d\phi(z(t))}{dt}$. Assuming harmonic oscillation of atoms of $z(t) = z_0 \cos \omega_z t$, where we take $z_0 = \sqrt{\hbar/m\omega_z}$ with m the atomic mass and $\omega_z = 2\pi \times 60$ kHz, the maximum frequency is estimated to be $\nu_r \approx 3.2$ kHz.

In the atom rest frame, the polarization rotation at ν_r can be viewed as the counter propagating σ^+ and σ^- waves at different frequencies $\nu_{\pm} = \nu_L \pm \nu_r$ with ν_L the frequency of the lattice laser. Near the magic frequency $\nu \approx \nu_L$, the corresponding light shift can be given by the sum of the differential light shift $\delta f(\nu_+) + \delta f(\nu_-)$, which is calculated to be ≈ 1 nHz for the $m_F = 9/2$ magnetic substate of ^{87}Sr with a total intensity of 25 kW/cm 2 . In particular, this effect is negligible when the quantization axis is parallel to the polarization rotating plane as the σ^{\pm} -polarized components of \mathbf{E}_L are nearly zero.

- [1] H. G. Dehmelt, IEEE Trans. Instrum. Meas. **IM-31**, 83 (1982).
 [2] P. Gill, Metrologia **42**, S125 (2005).
 [3] S. Bize *et al.*, J. Phys. B **38**, S449 (2005).
 [4] T. P. Heavner, S. R. Jefferts, E. A. Donley, J. H. Shirley, and T. E. Parker, Metrologia **42**, 411 (2005).

- [5] T. Rosenband *et al.*, Science **319**, 1808 (2008).
 [6] H. Katori, in *Proceedings of the 6th Symposium on Frequency Standards and Metrology*, edited by P. Gill (World Scientific, Singapore, 2002) p. 323.
 [7] H. Katori, M. Takamoto, V. G. Pal'chikov, and V. D. Ovsinnikov, Phys. Rev. Lett. **91**, 173005 (2003).

- [8] H. Katori, K. Hashiguchi, E. Y. Il'ina, and V. D. Ovsiannikov, *Phys. Rev. Lett.* **103**, 153004 (2009).
- [9] M. Takamoto and H. Katori, *Phys. Rev. Lett.* **91**, 223001 (2003).
- [10] M. Takamoto, F. L. Hong, R. Higashi, and H. Katori, *Nature (London)* **435**, 321 (2005).
- [11] A. D. Ludlow, M. M. Boyd, T. Zelevinsky, S. M. Foreman, S. Blatt, M. Notcutt, T. Ido, and J. Ye, *Phys. Rev. Lett.* **96**, 033003 (2006).
- [12] R. L. LeTargat, X. Baillard, M. Fouché, A. Bruschi, O. Tcherbakoff, G. D. Rovera, and P. Lemonde, *Phys. Rev. Lett.* **97**, 130801 (2006).
- [13] M. Takamoto, F. L. Hong, R. Higashi, Y. Fujii, M. Imae, and H. Katori, *J. Phys. Soc. Jpn.* **75**, 104302 (2006).
- [14] X. Baillard *et al.*, *Eur. Phys. J. D* **48**, 11 (2008).
- [15] G. K. Campbell *et al.*, *Metrologia* **45**, 539 (2008).
- [16] N. D. Lemke, A. D. Ludlow, Z. W. Barber, T. M. Fortier, S. A. Diddams, Y. Jiang, S. R. Jefferts, T. P. Heavner, T. E. Parker, and C. W. Oates, *Phys. Rev. Lett.* **103**, 063001 (2009).
- [17] T. Kohno, M. Yasuda, K. Hosaka, H. Inaba, Y. Nakajima, and F. Hong, *Appl. Phys. Express* **2**, 072501 (2009).
- [18] Z. W. Barber, C. W. Hoyt, C. W. Oates, L. Hollberg, A. V. Taichenachev, and V. I. Yudin, *Phys. Rev. Lett.* **96**, 083002 (2006).
- [19] X. Baillard, M. Fouché, R. L. LeTargat, P. G. Westergaard, A. Lecallier, Y. L. Coq, G. D. Rovera, S. Bize, and P. Lemonde, *Opt. Lett.* **32**, 1812 (2007).
- [20] N. Poli *et al.*, *Phys. Rev. A* **77**, 050501(R) (2008).
- [21] C. Lisdat, J. S. R. Vellore Winfred, T. Middelmann, F. Riehle, and U. Sterr, *Phys. Rev. Lett.* **103**, 090801 (2009).
- [22] F. L. Hong *et al.*, *Opt. Lett.* **34**, 692 (2009).
- [23] K. Gibble and B. J. Verhaar, *Phys. Rev. A* **52**, 3370 (1995).
- [24] S. Gupta, Z. Hadzibabic, M. W. Zwierlein, C. A. Stan, K. Dieckmann, C. H. Schunck, E. G. M. van Kempen, B. J. Verhaar, and W. Ketterle, *Science* **300**, 1723 (2003).
- [25] G. K. Campbell *et al.*, *Science* **324**, 360 (2009).
- [26] M. Takamoto and H. Katori, *J. Phys. Soc. Jpn.* **78**, 013301 (2009).
- [27] K. Gibble, *Phys. Rev. Lett.* **103**, 113202 (2009).
- [28] A. V. Taichenachev, V. I. Yudin, C. W. Oates, C. W. Hoyt, Z. W. Barber, and L. Hollberg, *Phys. Rev. Lett.* **96**, 083001 (2006).
- [29] V. D. Ovsiannikov, V. G. Pal'chikov, A. V. Taichenachev, V. I. Yudin, H. Katori, and M. Takamoto, *Phys. Rev. A* **75**, 020501(R) (2007).
- [30] A. V. Taichenachev, V. I. Yudin, and C. W. Oates, *Phys. Rev. A* **76**, 023806 (2007).
- [31] T. Akatsuka, M. Takamoto, and H. Katori, *Nat. Phys.* **4**, 954 (2008).
- [32] Y. Takasu, K. Maki, K. Komori, T. Takano, K. Honda, M. Kumakura, T. Yabuzaki, and Y. Takahashi, *Phys. Rev. Lett.* **91**, 040404 (2003).
- [33] S. Kraft, F. Vogt, O. Appel, F. Riehle, and U. Sterr, *Phys. Rev. Lett.* **103**, 130401 (2009).
- [34] Y. N. Martinez de Escobar, P. G. Mickelson, M. Yan, B. J. DeSalvo, S. B. Nagel, and T. C. Killian, *Phys. Rev. Lett.* **103**, 200402 (2009).
- [35] S. Stellmer, M. K. Tey, B. Huang, R. Grimm, and F. Schreck, *Phys. Rev. Lett.* **103**, 200401 (2009).
- [36] M. Greiner, O. Mandel, T. Esslinger, T. Hänsch, and I. Bloch, *Nature (London)* **415**, 39 (2002).
- [37] M. Takamoto, H. Katori, S. I. Marmo, V. D. Ovsiannikov, and V. G. Pal'chikov, *Phys. Rev. Lett.* **102**, 063002 (2009).
- [38] A. Hemmerich and T. W. Hänsch, *Phys. Rev. Lett.* **68**, 1492 (1992).
- [39] A. Rauschenbeutel, H. Schadwinkel, V. Gomer, and D. Meschede, *Opt. Commun.* **148**, 45 (1998).
- [40] H. Katori, T. Ido, Y. Isoya, and M. Kuwata-Gonokami, *Phys. Rev. Lett.* **82**, 1116 (1999).
- [41] P. Lemonde and P. Wolf, *Phys. Rev. A* **72**, 033409 (2005).
- [42] T. Ido and H. Katori, *Phys. Rev. Lett.* **91**, 053001 (2003).
- [43] T. Ido, Y. Isoya, and H. Katori, *Phys. Rev. A* **61**, 061403(R) (2000).
- [44] M. Yasuda, T. Kishimoto, M. Takamoto, and H. Katori, *Phys. Rev. A* **73**, 011403(R) (2006).
- [45] M. Notcutt, L. S. Ma, J. Ye, and J. L. Hall, *Opt. Lett.* **30**, 1815 (2005).
- [46] L. S. Ma, P. Jungner, J. Ye, and J. L. Hall, *Opt. Lett.* **19**, 1777 (1994).
- [47] E. Peik, T. Schneider, and C. Tamm, *J. Phys. B* **39**, 145 (2006).
- [48] G. J. Dick, J. D. Prestage, C. A. Greenhall, and L. Maleki, in *22nd Precise Time and Time Interval (PTTI) Applications and Planning Meeting* edited by R. L. Sydner (NASA Goddard Space Flight Center, Greenbelt, Maryland, 1991), pp. 487–508.
- [49] G. Santarelli, C. Audoin, A. Makdissi, P. Laurent, G. J. Dick, and A. Clairon, *IEEE Trans. Ultrason. Ferroelectr. Freq. Control* **45**, 887 (1998).
- [50] A. Quessada, R. P. Kovacich, I. Courtillot, A. Clairon, G. Santarelli, and P. Lemonde, *J. Opt. B* **5**, S150 (2003).
- [51] K. Numata, A. Kemery, and J. Camp, *Phys. Rev. Lett.* **93**, 250602 (2004).
- [52] A. D. Ludlow, X. Huang, M. Notcutt, T. Zanon-Willette, S. M. Foreman, M. M. Boyd, S. Blatt, and J. Ye, *Opt. Lett.* **32**, 641 (2007).
- [53] R. Long, A. K. Tuchman, and M. A. Kasevich, *Opt. Lett.* **32**, 2502 (2007).
- [54] I. J. Ma, J. Mertens, G. Z. Putlitz, and G. Schütte, *Z. Phys.* **208**, 266 (1968).
- [55] A. D. Ludlow *et al.*, *Science* **319**, 1805 (2008).
- [56] H. G. C. Werij, C. H. Greene, C. E. Theodosiou, and A. Gallagher, *Phys. Rev. A* **46**, 1248 (1992).
- [57] I. Courtillot, A. Quessada-Vial, A. Bruschi, D. Kolker, G. D. Rovera, and P. Lemonde, *Eur. Phys. J. D* **33**, 161 (2005).
- [58] A. Bruschi, R. L. LeTargat, X. Baillard, M. Fouché, and P. Lemonde, *Phys. Rev. Lett.* **96**, 103003 (2006).
- [59] J. Dalibard and C. Cohen-Tannoudji, *J. Opt. Soc. Am. B* **6**, 2023 (1989).
- [60] P. J. Windpassinger, D. Oblak, P. G. Petrov, M. Kubasik, M. Saffman, C. L. Garrido Alzar, J. Appel, J. H. Müller, N. Kjaergaard, and E. S. Polzik, *Phys. Rev. Lett.* **100**, 103601 (2008).
- [61] J. Lodewyck, P. G. Westergaard, and P. Lemonde, *Phys. Rev. A* **79**, 061401(R) (2009).
- [62] M. Schleier-Smith, I. Leroux, and V. Vuletic, *Arxiv preprint arXiv:0810.2582* (2008).